# Asymmetrical Aircraft Response to Dryden Turbulence Model

AE4304P: Stochastic Aerospace Systems Practical

Richard Henry Adam
[redacted]

March 25, 2025

# Contents

**1 Introduction** **2**

**2 Aircraft Model and Stability Analysis** **3**
2.1 State-Space Representation . . . . . 3
2.2 Stability Analysis and Controller Design . . . . . 4

**3 Time-Domain Analysis** **5**
3.1 Lateral Acceleration Integration . . . . . 5
3.2 Simulation Results . . . . . 5
3.3 Time-Domain Simulation Analysis . . . . . 7

**4 Spectral Analysis** **8**
4.1 Spectral Analysis Results . . . . . 8
4.2 Differences Between Horizontal and Vertical Gusts . . . . . 11
4.3 Calculation-Based Changes in PSD . . . . . 11

**5 Variance Analysis** **12**
5.1 Variance Results . . . . . 12
5.2 Variance in Horizontal vs Vertical Turbulence . . . . . 12
5.3 Variance in Experimental vs Analytical Models . . . . . 13

**6 Conclusion** **13**

**A Stability Derivatives and Landing Condition** **15**

**B MATLAB Code** **16**

# 1 Introduction

When designing an aircraft, it is critical to analyze its response to atmospheric turbulence and ensure its safety across multiple different flight conditions. Asymmetrical turbulence, or turbulence that does not act constantly across a specific aircraft axis, is especially important as it can create heavy aerodynamic loads, high deflections, and strong vibrations. The objective of this assignment is to analyze the asymmetric lateral and vertical turbulence response of a Cessna Citation I in its landing condition with relatively low speed and relatively low altitude. To do this, the Dryden spectral model of turbulence is employed for modeling wind gust disturbances. The aircraft equations of motion, augmented with the Dryden model, are derived and simulated for both horizontal and vertical turbulence cases in the following two conditions:

- Horizontal turbulence: $L_g = 150\,\text{m}$, $\sigma_{u_g} = 3\,\text{m/s}$
- Vertical turbulence: $L_g = 150\,\text{m}$, $\sigma_{w_g} = 2\,\text{m/s}$

Depictions of asymmetric horizontal and vertical turbulence can be seen in Figures 1a and 1b respectively.[1]

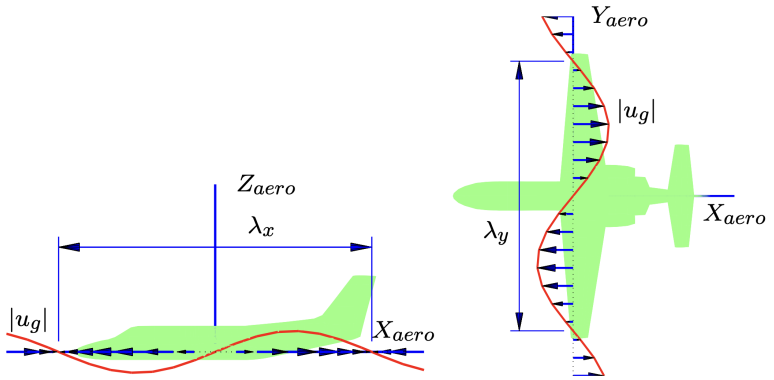


(a) Depiction of asymmetric horizontal(lateral) turbulence on an aircraft

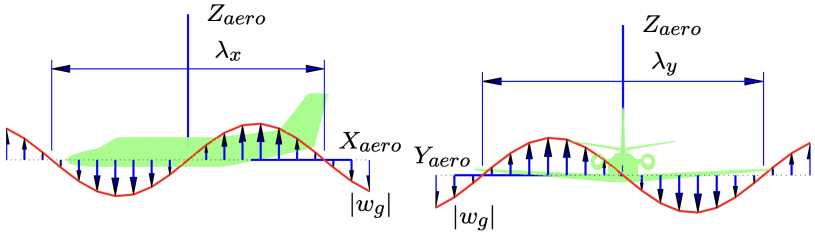


(b) Depiction of asymmetric vertical turbulence on an aircraft

Figure 1: Graphic of asymmetric turbulence types to be modeled

The analysis of these two turbulence conditions comprises of four main areas:

1. A stability analysis of the aircraft using its state-space representation and the design of a simple roll-damper controller.
2. Time-domain simulations and analysis of the aircraft response to stochastic turbulence inputs.
3. Spectral analysis to compute the power spectral densities (PSDs) analytically and experimentally via FFT and a smoothing filter.

4. Variance estimation of the aircraft states using analytical integration, experimental PSDs, and the MATLAB `var` function.

Because the simulations for horizontal and vertical turbulence are conducted separately, each of these analyses is split into horizontal and vertical responses.

# 2 Aircraft Model and Stability Analysis

## 2.1 State-Space Representation

The Citation's asymetric equations of motion, augmented with the Dryden model, can be represented in state-space form:

$$\dot{x} = Ax + Bu,$$

with the state vector:

$$x = \begin{bmatrix} \beta & \varphi & \frac{pb}{2V} & \frac{rb}{2V} & u_g & u_g^* & \alpha_g & \alpha_g^* & \beta_g & \beta_g^* \end{bmatrix}^T$$

and the input vector:

$$u = \begin{bmatrix} \delta_a & \delta_r & w_1 & w_3 & w_2 \end{bmatrix}^T.$$

Where $\beta$ is the side-slip angle in radians, $\varphi$ is the roll angle in radians, $\frac{pb}{2V}$ is the normalized roll rate, $\frac{rb}{2V}$ is the normalized yaw rate, $u_g$ and $u_g^*$ is the longitudinal gust velocity in m/s and its unitless counterpart, $\alpha_g$ and $\alpha_g^*$ is the angle of attack gust velocity in m/s and its unitless counterpart, and $\beta_g$ and $\beta_g^*$ is the side-slip gust velocity in m/s and its unitless counterpart. In the input vector, $\delta_a$ is aileron deflection, $\delta_a$ is aileron deflection, and $w_1, w_2$, and $w_3$ are the white noise inputs for longitudinal, vertical, and lateral gusts respectively.

It is important to note that, in some models, the state variables are reduced to the first four - $\beta$, $\varphi$, $\frac{pb}{2V}$, and $\frac{rb}{2V}$ - and the gust variables are abandoned. The time and spectral analysis will only regard these first four states, but the full equation is used in order to conduct the variance analysis on the gust variables in the final section. In addition, this model includes augmentation by the Dryden model which has the following relationships in state-space for horizontal($u_g$) and vertical($w_g$) turbulence:[2]

$$\dot{u}_g(t) = -\frac{V}{L_g} u_g(t) + \sigma_{u_g} \sqrt{\frac{2V}{L_g}} w_1(t) \tag{1}$$

$$\begin{bmatrix} \dot{w}_g(t) \\ \dot{w}_g^*(t) \end{bmatrix} = \begin{bmatrix} 0 & 1 \\ -\frac{V^2}{L_g^2} & -\frac{2V}{L_g} \end{bmatrix} \begin{bmatrix} w_g(t) \\ w_g^*(t) \end{bmatrix} + \begin{bmatrix} \sigma_{w_g} \sqrt{\frac{3V}{L_g}} \\ (1 - 2\sqrt{3}) \sigma_{w_g} \sqrt{\left(\frac{V}{L_g}\right)^3} \end{bmatrix} w_3(t) \tag{2}$$

After augmentation with the Dryden model equations 1 and 2 and derivations using provided stability derivatives in Appendix A, the matrices $A$ and $B$ are as follows:

$$A = \begin{bmatrix} -0.1731 & 0.1987 & -0.0152 & -7.6194 & 0 & 0 & 0 & 0 & -0.1731 & 0 \\ 0 & 0 & 7.6946 & 0 & 0 & 0 & 0 & 0 & 0 & 0 \\ -0.5029 & 0 & -2.5153 & 2.0041 & -1.4412 & 0 & -2.0126 & 0 & -0.5029 & 0 \\ 0.3575 & 0 & -0.1615 & -0.3478 & 0.0133 & 0 & -0.1318 & 0 & 0.3575 & 0 \\ 0 & 0 & 0 & 0 & 0 & 1.0000 & 0 & 0 & 0 & 0 \\ 0 & 0 & 0 & 0 & -2.1603 & -4.1057 & 0 & 0 & 0 & 0 \\ 0 & 0 & 0 & 0 & 0 & 0 & 0 & 1.0000 & 0 & 0 \\ 0 & 0 & 0 & 0 & 0 & 0 & -5.9967 & -6.7955 & 0 & 0 \\ 0 & 0 & 0 & 0 & 0 & 0 & 0 & 0 & 0 & 1.0000 \\ 0 & 0 & 0 & 0 & 0 & 0 & 0 & 0 & -0.1174 & -0.6853 \end{bmatrix}$$

$$B = \begin{bmatrix} 0 & 0.0531 & 0 & 0 & 0 \\ 0 & 0 & 0 & 0 & 0 \\ -1.7158 & 0.1602 & 0 & 0 & 0 \\ -0.0252 & -0.2893 & 0 & 0 & 0 \\ 0 & 0 & 0.0408 & 0 & 0 \\ 0 & 0 & -0.1339 & 0 & 0 \\ 0 & 0 & 0 & 0.0523 & 0 \\ 0 & 0 & 0 & -0.2752 & 0 \\ 0 & 0 & 0 & 0 & 0.0395 \\ 0 & 0 & 0 & 0 & -0.0192 \end{bmatrix}$$

### 2.2 Stability Analysis and Controller Design

Before a time domain and spectral analysis can be conducted, the system must be stable. To check this, the eigenvalues of the uncontrolled system are determined and are shown to be:

$$\text{-2.63,} \quad \text{-0.25} \pm \text{1.82i,} \quad \text{0.093,} \quad \text{-0.62,} \quad \text{-3.49,} \quad \text{-1.04,} \quad \text{-5.75,} \quad \text{-0.34,} \quad \text{-0.34}$$

The positive eigenvalue indicates that the plane will be unstable without any stability augmentation. To remedy this, a roll damper is designed using the control law:

$$\delta_a = K_\varphi \varphi + K_p p,$$

The gains are tuned via an optimization algorithm that solves for stable poles with the highest damping ratio, resulting in the gains $K_\varphi = -0.4154$ and $K_p = 0.1151$. With the roll-damper at these gains, the eigenvalues of the system are:

$$\text{-0.65} \pm \text{1.69i} \quad \text{-0.77} \pm \text{1.98i} \quad \text{-0.61} \quad \text{-3.49} \quad \text{-1.04} \quad \text{-5.75} \quad \text{-0.34} \quad \text{-0.34}$$

The positive eigenvalue has clearly been shifted to the left-half plane, and the Cessna is now stable, so a time and spectral domain analyses can now be conducted on the damped system.

# 3 Time-Domain Analysis

Time-domain simulations were performed to generate measurements of the Citation's response to the two turbulence conditions. Both horizontal and vertical simulations were driven by a white-noise input generated using MATLAB's randn() function.

## 3.1 Lateral Acceleration Integration

It is important that the lateral accelerations be accounted for in aircraft analysis, as it represents the lateral aerodynamic loading of the plane. The lateral acceleration was calculated using the relation:[3]

$$a_y = V(\dot{\psi} + \dot{\beta}) \tag{3}$$

The linearized asymmetric equations of motion[4] show that

$$\dot{\psi} = \frac{1}{cos(\theta_0)} r \tag{4}$$

and with $\theta_0$ equal to zero in this case, the equation can be shown as:

$$a_y = V(r + \dot{\beta}) \tag{5}$$

To add $a_y$ as a state, the A matrix was augmented by adding a row made up of the first row($\dot{\beta}$) plus the $r$ term multiplied by V. In addition, the C-matrix was chosen to convert the time series data to more interpretable units, so all angle values are scaled by $\frac{180}{pi}$ to convert to degrees and the normalized rates are scaled by $\frac{2V}{b}\frac{180}{pi}$ to convert to degrees per second. The D matrix consists of all zeros, as the system must be causal.

After augmenting, the time response of all state variables are recorded with simulations spanning two minutes (120s) to balance time-domain legibility with frequency-domain accuracy.

## 3.2 Simulation Results

Figures 2 and 3 show time responses of all aircraft states for horizontal and vertical turbulence, respectively.

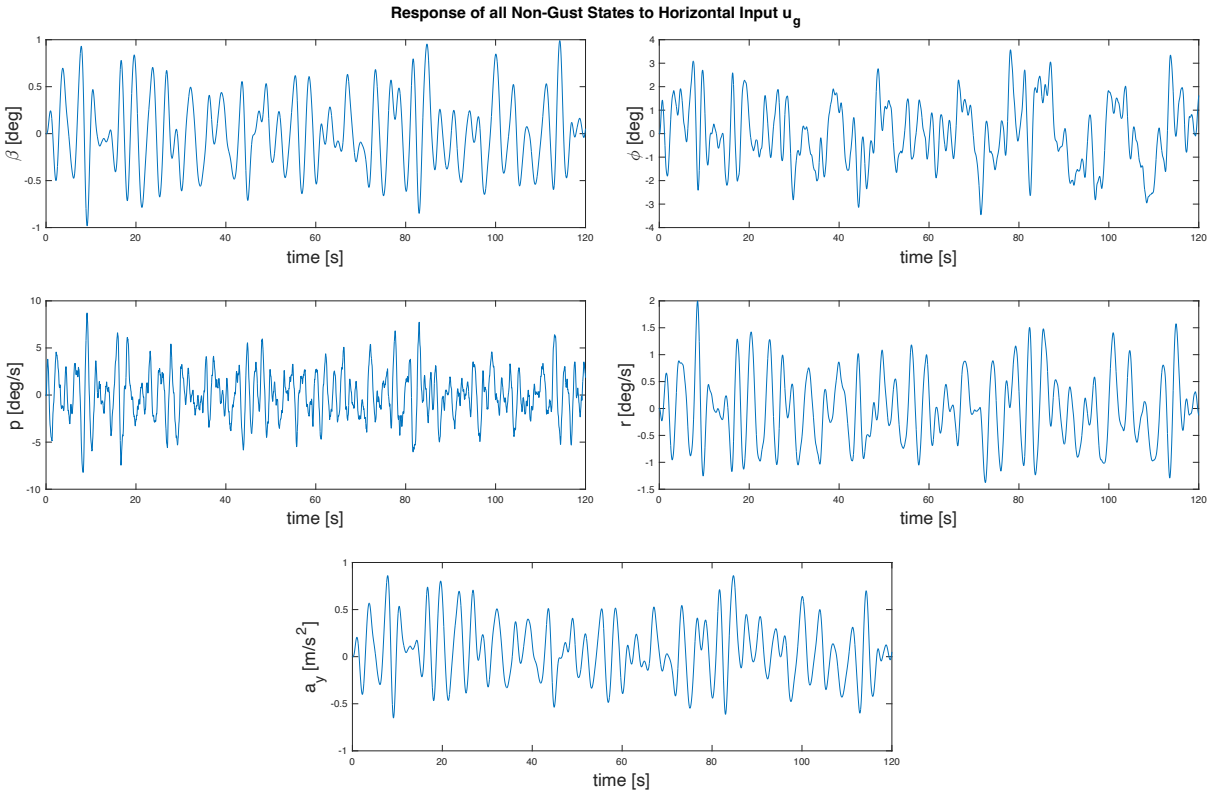


Figure 2: Time-domain response of all aircraft states (including lateral acceleration) to horizontal turbulence.

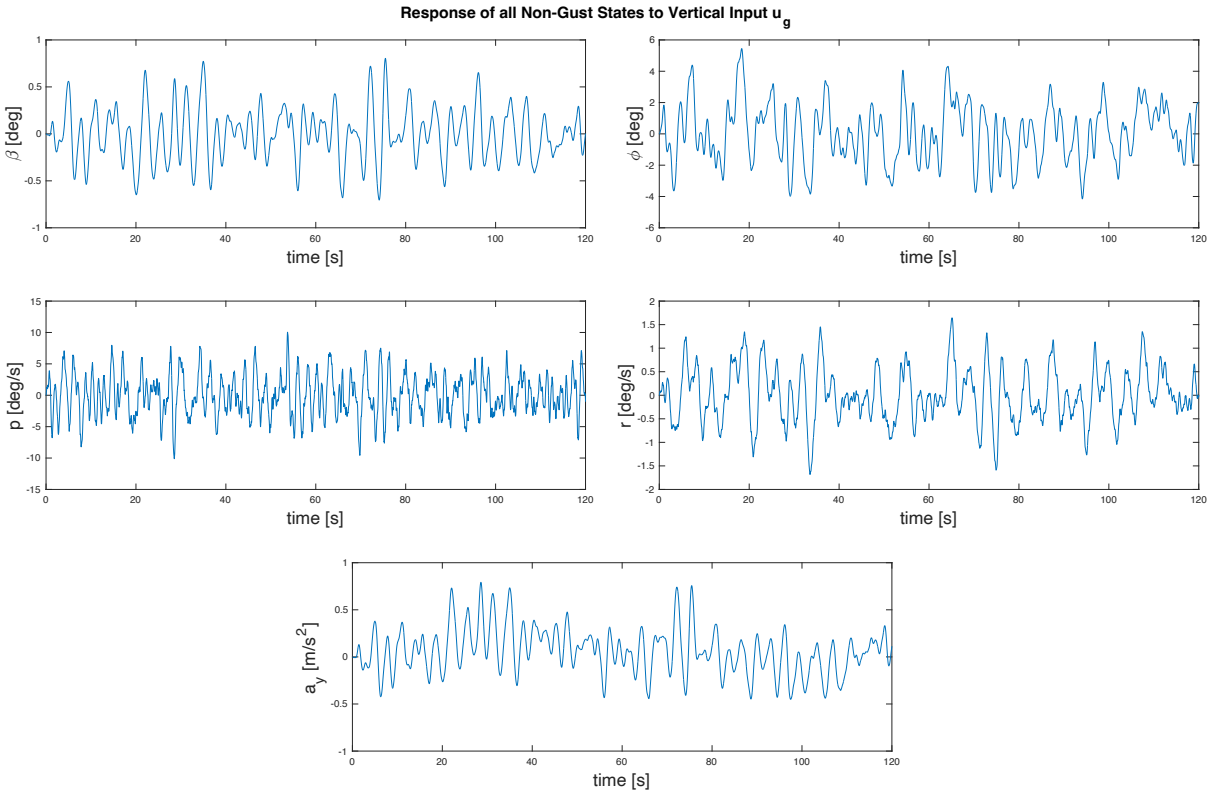


Figure 3: Time-domain response of all aircraft states (including lateral acceleration) to vertical turbulence.

### 3.3 Time-Domain Simulation Analysis

In Figure 2, it can be seen that all of the state-variables are bounded zero-mean signals, so the roll-damper has clearly worked to stabilize the system. Across both horizontal and vertical tests, the highest angle $\beta$ is 0.99deg, the highest angle $\varphi$ is 5.45deg, the highest value of p is 10.1deg/s, the highest r is 2.0deg/s, and the highest lateral acceleration is 0.86m/s$^2$. The side-slip angle $\beta$ and yaw rate r are both very low, but the roll $\varphi$ and roll rate p are both somewhat concerning, as a 5.45deg roll or temporary 10deg/s roll rate can be significant while landing an aircraft. One way to address this is by incorporating a more effective roll-damper system. On the positive side for stability the max lateral acceleration of 0.86m/s$^2$ is unlikely to be disruptive during landing, and over the short periods during which the acceleration is experienced, it will not significantly impact landing position or cross passenger comfort thresholds. Along with the time domain analysis, it is prudent to conduct a spectral analysis of these states to analyze them in the frequency domain.

# 4 Spectral Analysis

Variance estimates for each non-gust aircraft state including lateral acceleration were obtained using three different methods:

1. **Analytical:** The PSD can be found analytically using MATLAB's `bode()` function. The `bode()` function outputs the magnitude response of the transfer function, $|H(j\omega)|$, so it can be squared to find the analytical PSD, which is defined as $|H(j\omega)|^2$.

2. **Experimental PSD by Fast Fourier Transform:** MATLAB's fast fourier transform function can be used to find the signal of a stochastic variable $\bar{x}[k]$ in frequency domain, X[k], which can then be applied to the equation

$$\hat{S}_{\bar{x}\bar{x}}(\omega) = \varphi_{N_{\bar{x}\bar{x}}} = \frac{1}{N} X^*[k]X[k] \tag{6}$$

   to estimate the auto-PSD of the given stochastic variable.

3. **Experimental PSDs by Smoothing Filter:** In addition to the fft-derived PSD, a smoothing filter was applied for a realization of the periodogram. A smoothing filter is generally used to reduce noise in a signal by replacing each point with a weighted average of points within a smoothing window. The smoothing filter applied in this case is shown here:

$$\varphi_{estimate}[k] = 0.25 * \varphi[k-1] + 0.5 * \varphi[k] + 0.25 * \varphi[k+1] \tag{7}$$

   Because this smoothing filter is essentially a convolution, MATLAB's `conv()` function can be used to calculate this from the periodogram found in the previous method.

## 4.1 Spectral Analysis Results

Figures 4a–4e illustrate the comparison between the analytical PSD and the experimental methods for the horizontal turbulence case.

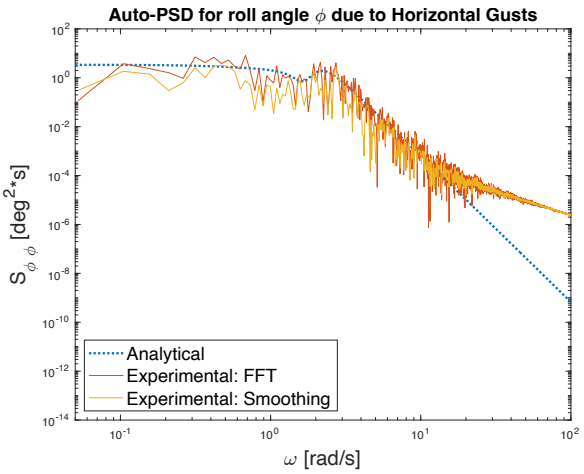


(a) Comparison of analytical, FFT, and smoothed PSD estimates for $\varphi$

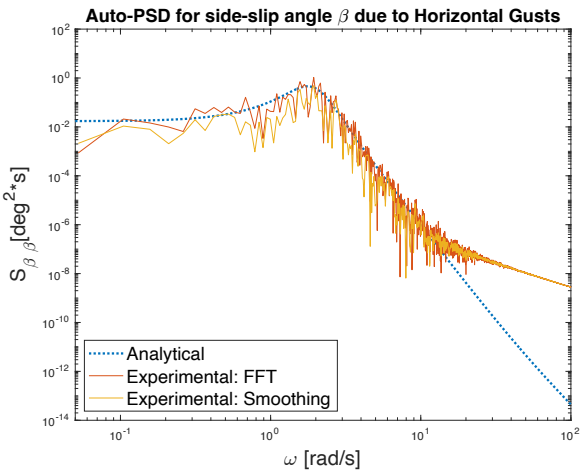


(b) Comparison of analytical, FFT, and smoothed PSD estimates for $\beta$

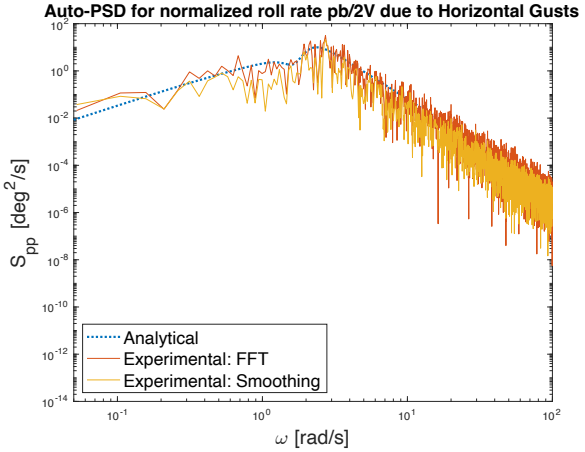


(c) Comparison of analytical, FFT, and smoothed PSD estimates for $p$

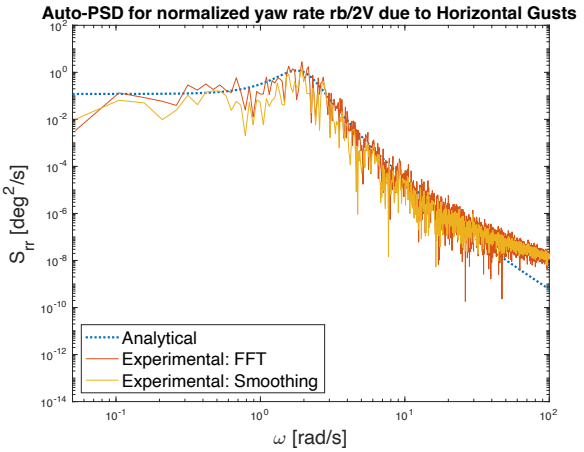


(d) Comparison of analytical, FFT, and smoothed PSD estimates for $r$

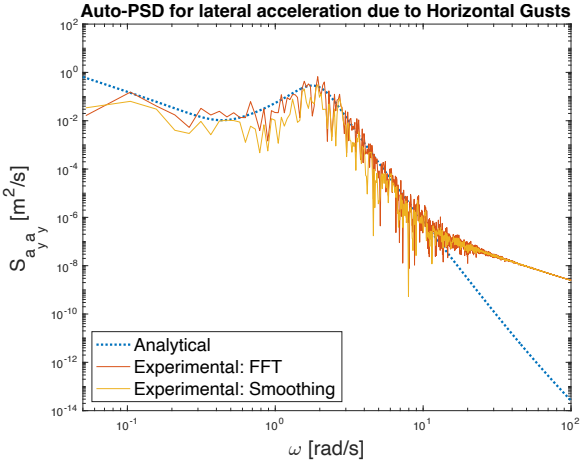


(e) Comparison of analytical, FFT, and smoothed PSD estimates for $a_y$

Figure 4: Comparative plots of analytical, FFT-derived, and smoothed estimates of power spectral density of each state for vertical gusts

In addition, the vertical turbulence cases can be seen in Figures 5a–5e.

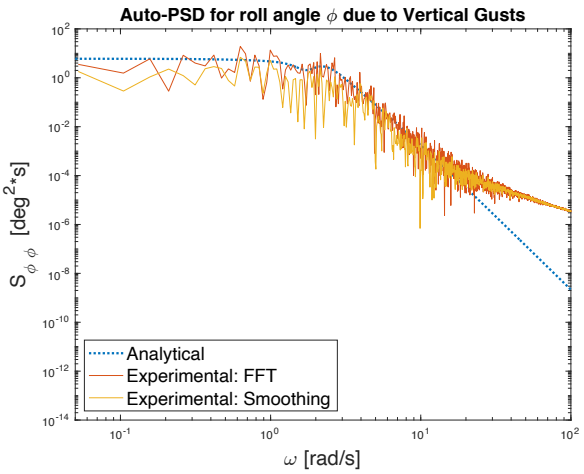


(a) Comparison of analytical, FFT, and smoothed PSD estimates for $\varphi$

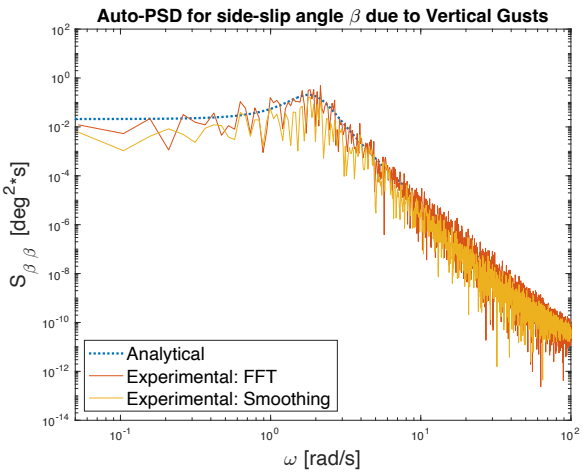


(b) Comparison of analytical, FFT, and smoothed PSD estimates for $\beta$

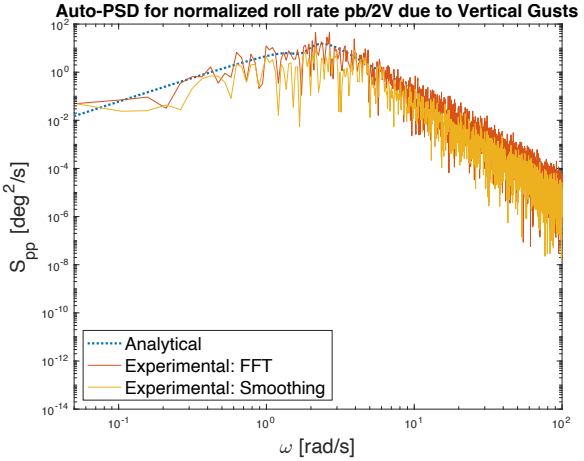


(c) Comparison of analytical, FFT, and smoothed PSD estimates for $p$

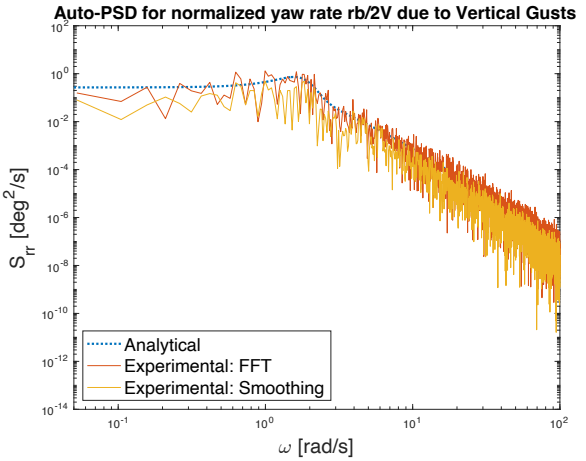


(d) Comparison of analytical, FFT, and smoothed PSD estimates for $r$

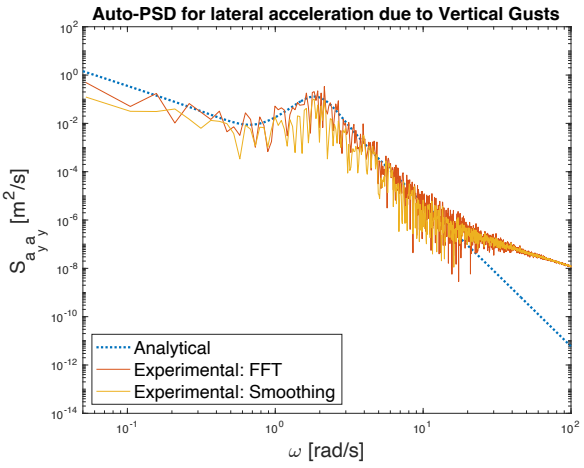


(e) Comparison of analytical, FFT, and smoothed PSD estimates for $a_y$

Figure 5: Comparative plots of analytical, FFT-derived, and smoothed estimates of power spectral density of each state for horizontal gusts

## 4.2 Differences Between Horizontal and Vertical Gusts

Although the responses of the states to horizontal and vertical turbulence share many properties in the frequency domain, there are some important differences. In the horizontal turbulence case, there is a slightly higher peak of the side-slip angle PSD $S_{\beta\beta}$ and a slightly more pronounced peak of its normalized yaw-rate auto-PSD, $S_{rr}$. Conversely, in the vertical case there is a slightly higher power of roll angle $\varphi$ at low frequencies. These findings agree with the fact that asymmetric horizontal gusts have a high effect on sideslip and yaw rate, while asymmetric vertical gusts have a high effect on roll and roll rate. The auto-psd of lateral acceleration is almost identical in the vertical and horizontal case, suggesting that there is not a large difference in how vertical and lateral gusts affect lateral acceleration in landing scenarios.

## 4.3 Calculation-Based Changes in PSD

Generally, the analytical, experimental, and smoothed PSDs share most characteristics, especially at lower frequencies. The smoothed PSD does fit the analytical expectations slightly better at low frequencies, and reduces noise in the signal as a smoothing filter should. At frequencies above 10rad/s, though, the experimental and smoothed estimates both diverge significantly from the analytical for multiple states in both horizontal and vertical turbulence. In both cases, variables diverge to have higher auto-PSDs at higher frequencies than is analytically expected. This suggests that the model fails to capture some of the high-frequency response in the aircraft system. One important finding is that the divergent variables change depending on which form of turbulence is simulated.

In the vertical case, only the experimental and smoothed auto-PSDs of $\varphi$ and $a_y$ diverge from the analytical, which occurs at frequencies above 10rad/s. It makes sense that there would be little divergence of $\beta$ and r with vertical turbulence, as the vertical turbulence model should not affect the sideslip or yaw rate.

On the other hand, the addition of horizontal turbulence sees the experimental auto-PSDs of roll angle $\varphi$, side-slip angle $\beta$, normalized yaw rate $r$ and lateral acceleration $a_y$ all diverge with the analytical at high frequencies. This means that the model does not adequately capture the relationship between high-frequency horizontal turbulence and the yaw behavior of the Citation. By examining the variance across the two situations, the differences between models can be examined more fully.

# 5 Variance Analysis

Using the auto-PSD estimates from the analytical, experimental, and smoothed derivations, the equation

$$\sigma_{\bar{x}}^2 = \frac{1}{\pi} \int S_{\bar{x}\bar{x}}(\omega) d\omega \tag{8}$$

can be applied to find the variance of each state variable. It is important to note that since the one-sided PSD is found instead of the full PSD, the integral is scaled by $\frac{1}{\pi}$ instead of $\frac{1}{2\pi}$. Since the computer uses discrete representations of the data, a trapezoidal sum was used to estimate the integral. The results for the variance calculation are compared for the auto-psd estimates alongside the variance found by applying MATLAB's `var()` function to the time signals of each state.

## 5.1 Variance Results

Tables 1 and 2 show the variance estimates for the horizontal and vertical cases respectively.

Table 1: Variance estimates for horizontal turbulence.

| State | Analytical | FFT | Smoothed | Function | Units |
|---|---|---|---|---|---|
| $\beta$ | 0.1614 | 0.1478 | 0.06000 | 0.1479 | $\text{deg}^2$ |
| $\varphi$ | 1.842 | 1.902 | 0.7617 | 1.902 | $\text{deg}^2$ |
| $p$ | 6.004 | 6.458 | 2.732 | 6.459 | $(\frac{deg}{s})^2$ |
| $r$ | 0.4596 | 0.4275 | 0.1741 | 0.4275 | $(\frac{deg}{s})^2$ |
| $a_y$ | 0.1110 | 0.09723 | 0.03985 | 0.09318 | $(\frac{m}{s^2})^2$ |
| $u_g$ | 0.8520 | 0.8639 | 0.3389 | 0.8796 | $\text{deg}^2$ |
| $u_g^*$ | 0.002550 | 0.002577 | 0.001008 | 0.002629 | - |

Table 2: Variance estimates for vertical turbulence.

| State | Analytical | FFT | Smoothed | Function | Units |
|---|---|---|---|---|---|
| $\beta$ | 0.08122 | 0.07837 | 0.02475 | 0.07837 | $\text{deg}^2$ |
| $\varphi$ | 3.621 | 3.441 | 1.228 | 3.440 | $\text{deg}^2$ |
| $p$ | 11.07 | 10.81 | 3.668 | 10.81 | $(\frac{deg}{s})^2$ |
| $r$ | 0.3512 | 0.3345 | 0.1138 | 0.3345 | $(\frac{deg}{s})^2$ |
| $a_y$ | 0.07879 | 0.06245 | 0.01902 | 0.05859 | $(\frac{m}{s^2})^2$ |
| $\alpha_g$ | 0.8832 | 0.8764 | 0.3302 | 0.8876 | $\text{deg}^2$ |
| $\alpha_g^*$ | 0.006510 | 0.006514 | 0.002451 | 0.006609 | - |

In each of these tables, all state variables not listed have variances of zero across all methods.

## 5.2 Variance in Horizontal vs Vertical Turbulence

The variance tables make it clear which variables the horizontal and vertical gusts affect most strongly. The horizontal turbulence has stronger effects on the $\beta$, r, $a_y$, $u_g$, and $u_g^*$ variables, while the vertical turbulence has the strongest effect on $\varphi$, p, $\alpha_g$, and $\alpha_g^*$. The gust variables are more obvious, but it is clear that asymmetrical horizontal gusts have the highest affect on the sideslip, yaw rate, and lateral loading, while asymmetrical vertical gusts affect the roll and roll rate most. This suggests that, in the landing configuration, the main driver for lateral acceleration is the yaw rate and induced sideslips. That being said, the variance of lateral

acceleration from vertical gusts is about 70% of the variance from horizontal gusts, so it cannot be ignored when considering the landing configuration.

### 5.3 Variance in Experimental vs Analytical Models

Though the analytical, fft-derived, and `var()`-derived variances all mostly agree, the smoothed periodogram estimates are all significantly lower than the others. This is because the smoothing filter, as a rolling weighted average, reduces the extremes in the set and decreases sample-to-sample variability. This confirms that, although the smoothed functions can help reduce signal noise, it does not properly represent the power of the signal. The fft-based and `var()`-derived variances match the best, often being the same until the fourth significant figure, while the analytical stays within 15% of the fft and `var()` results. This is expected as the fft and the var() function are both derived directly from the time series itself, whereas the analytical is related to the state-space equation that generated the time series.

## 6 Conclusion

This study provides valuable insights into the asymmetrical response of a Cessna Citation I to atmospheric turbulence during landing conditions. Through comprehensive analysis using the Dryden spectral model, we have characterized the aircraft's behavior under both horizontal and vertical turbulence conditions.

The stability analysis revealed an initially unstable system that was successfully stabilized through the implementation of a roll-damper controller with optimized gains ($K_\varphi$ = -0.4154, $K_P$ = 0.1151). The controller is critical initial step in turbulence response analysis, as it plays a large role in disturbance rejection.

Time-domain analysis demonstrated that while most state variables remained well within acceptable limits, roll angle (reaching 5.45°) and roll rate (peaking at 10°/s) reached potentially concerning values during landing scenarios. These findings suggest that a more robust roll-damper system may be beneficial for improving landing safety under turbulent conditions. In addition, the maximum lateral acceleration of 0.86 m/s² is not severe, and likely will not affect landing precision and passenger comfort while landing.

The spectral analysis revealed distinct differences in aircraft response to horizontal versus vertical turbulence. As expected, horizontal gusts predominantly affected sideslip angle ($\beta$), yaw rate (r), and lateral acceleration ($a_y$), while vertical gusts had stronger effects on roll angle ($\varphi$) and roll rate (p). This asymmetrical response pattern aligns with aerodynamic theory and provides validation for our modeling approach.

Notably, our analytical models showed good agreement with simulated "experimental" data at lower frequencies but diverged significantly at frequencies above 10 rad/s. The divergence was seen most clearly in the states directly affected by the horizontal and vertical gusts respectively, suggesting limitations in the model's ability to capture high-frequency plane behavior under wind gusts.

Variance analysis further confirmed how different turbulence types affect aircraft states differently. In terms of derivation methodology, the close alignment between FFT-derived and time-domain variance estimates validates our frequency-domain approach, while the discrepancy with smoothed periodogram estimates highlights the limitations of aggressive noise filtering in preserving signal power characteristics. From an operational perspective, these findings emphasize the importance of considering asymmetrical turbulence affects in aircraft design and control system development, particularly for landing scenarios where stability margins are reduced. Overall, while analytical methods can help design aircraft, it is important to examine the experimental findings under turbulent conditions and to have a turbulence model that captures as much of the response as possible.

Future work should focus on testing models to more accurately represent the high-frequency response of the Citation to turbulence as well as implementing a more sophisticated control system for the roll damping.

## References


[1] M. Mulder, "Stochastic aerospace systems lecture slides," 2025, lecture Slides 1-7, AE4304, Delft University of Technology.

[2] J. A. Mulder, J. C. V. der Vaart, W. H. J. J. V. Staveren, Q. P. Chu, and M. Mulder, "Aircraft responses to atmospheric turbulence," 2025, lecture Notes AE4304, Delft University of Technology.

[3] E. Smeur, "Stochastic aerospace systems practical instructions," 2025, aE4304P, Delft University of Technology.

[4] J. A. Mulder, W. H. J. J. V. Staveren, J. C. V. der Vaart, and E. D. Weerdt, "Flight dynamics," 2025, lecture Notes AE3302, Delft University of Technology.

# A Stability Derivatives and Landing Condition

**Aircraft :** Cessna Ce500 Citation I

**Configuration :** landing

| | | | | | | | | | | |
|---|---|---|---|---|---|---|---|---|---|---|
| $x_{c.g.}$ | = | 0.30 | c̄ | | | | | | | |
| $W$ | = | 44675 | N | $V$ | = | 51.4 | m/sec | $\mu_b$ | = | 11 |
| $m$ | = | 4556 | kg | $h$ | = | 0 | m | $K_X^2$ | = | 0.012 |
| $S$ | = | 24.2 | $m^2$ | $\rho$ | = | 1.225 | $kg/m^3$ | $K_Z^2$ | = | 0.037 |
| $\bar{c}$ | = | 2.022 | m | $\mu_c$ | = | 76 | | $K_{XZ}$ | = | 0.002 |
| $b$ | = | 13.36 | m | $l_h$ | = | 5.5 | m | $K_Y^2$ | = | 0.980 |
| $C_{X_0}$ | = | 0 | | $C_{Z_0}$ | = | -1.1360 | | | | |
| $C_{X_u}$ | = | -0.2173 | | $C_{Z_u}$ | = | -2.2720 | | $C_{m_u}$ | = | 0 |
| $C_{X_\alpha}$ | = | 0.4692 | | $C_{Z_\alpha}$ | = | -5.1300 | | $C_{m_\alpha}$ | = | -0.4000 |
| | | | | $C_{Z_{\dot{\alpha}}}$ | = | -1.4050 | | $C_{m_{\dot{\alpha}}}$ | = | -3.6150 |
| $C_{X_q}$ | = | 0 | | $C_{Z_q}$ | = | -3.8400 | | $C_{m_q}$ | = | -7.3500 |
| $C_{X_\delta}$ | = | 0 | | $C_{Z_\delta}$ | = | -0.6238 | | $C_{m_\delta}$ | = | -1.5530 |
| $C_{Y_\beta}$ | = | -0.9896 | | $C_{\ell_\beta}$ | = | -0.0772 | | $C_{n_\beta}$ | = | 0.1628 |
| $C_{Y_p}$ | = | -0.0870 | | $C_{\ell_p}$ | = | -0.3415 | | $C_{n_p}$ | = | -0.0108 |
| $C_{Y_r}$ | = | 0.4300 | | $C_{\ell_r}$ | = | 0.2830 | | $C_{n_r}$ | = | -0.1930 |
| $C_{Y_{\delta_a}}$ | = | 0 | | $C_{\ell_{\delta_a}}$ | = | -0.2349 | | $C_{n_{\delta_a}}$ | = | 0.0286 |
| $C_{Y_{\delta_r}}$ | = | 0.3037 | | $C_{\ell_{\delta_r}}$ | = | 0.0286 | | $C_{n_{\delta_r}}$ | = | -0.1261 |

# B MATLAB Code

The MATLAB code used for control, simulation, and analysis is provided in the files:

1. `code_for_report_final.m`
2. `cesna_variables.m`

included in the provided zip file.